

000 054
 001 055
 002 056
 003 057
 004 058
 005 059
 006 060
 007 061
 008 062
 009 063
 010 064
 011 065
 012 066
 013 067
 014 068
 015 069
 016 070
 017 071
 018 072
 019 073
 020 074
 021 075
 022 076
 023 077
 024 078
 025 079
 026 080
 027 081
 028 082
 029 083
 030 084
 031 085
 032 086
 033 087
 034 088
 035 089
 036 090
 037 091
 038 092
 039 093
 040 094
 041 095
 042 096
 043 097
 044 098
 045 099
 046 100
 047 101
 048 102
 049 103
 050 104
 051 105
 052 106
 053 107

Supplementary Material to “External Prior Guided Internal Prior Learning for Real Noisy Image Denoising”

Anonymous CVPR submission

Paper ID 1047

In this supplementary material, we provide:

1. The closed-form solution of the sparse coding problem (6) in the main paper.
2. More denoising results on the real noisy images in dataset [1].
3. More denoising results on the 15 cropped real noisy images (with mean image of 500 shots as “ground truth”) in dataset [2].
4. More denoising results on the 60 cropped real noisy images (with mean image of 500 shots as “ground truth”) from dataset [2].

1. Closed-Form Solution of the Weighted Sparse Coding Problem (6)

For notation simplicity, we ignore the indices n, m, t in problem (6) of the main paper. It turns into the following weighted sparse coding problem:

$$\min_{\alpha} \|\mathbf{y} - \mathbf{D}\alpha\|_2^2 + \sum_{j=1}^{3p^2} \lambda_j |\alpha_j|. \quad (1)$$

Since \mathbf{D} is an orthogonal matrix, problem (1) is equivalent to

$$\min_{\alpha} \|\mathbf{D}^T \mathbf{y} - \alpha\|_2^2 + \sum_{j=1}^{3p^2} \lambda_j |\alpha_j|. \quad (2)$$

For simplicity, we denote $\mathbf{z} = \mathbf{D}^T \mathbf{y}$. Here we have $\lambda_j > 0, j = 1, \dots, 3p^2$, then problem (2) can be written as

$$\min_{\alpha} \sum_{j=1}^{3p^2} ((\mathbf{z}_j - \alpha_j)^2 + \lambda_j |\alpha_j|). \quad (3)$$

The problem (3) is separable w.r.t. each α_j and hence can be simplified to $3p^2$ independent scalar minimization problems

$$\min_{\alpha_j} (\mathbf{z}_j - \alpha_j)^2 + \lambda_j |\alpha_j|, \quad (4)$$

where $j = 1, \dots, 3p^2$. Taking derivative of α_j in problem (4) and setting the derivative to be zero. There are two cases for the solution.

(a) If $\alpha_j \geq 0$, we have

$$2(\alpha_j - \mathbf{z}_j) + \lambda_j = 0. \quad (5)$$

The solution is

$$\hat{\alpha}_j = \mathbf{z}_j - \frac{\lambda_j}{2} \geq 0. \quad (6)$$

So $\mathbf{z}_j \geq \frac{\lambda_j}{2} > 0$, and the solution $\hat{\alpha}_j$ can be written as

$$\hat{\alpha}_j = \text{sgn}(\mathbf{z}_j) * (|\mathbf{z}_j| - \frac{\lambda_j}{2}), \quad (7)$$

where $\text{sgn}(\bullet)$ is the sign function.

(b) If $\alpha_j < 0$, we have

$$2(\alpha_j - \mathbf{z}_j) - \lambda_j = 0. \quad (8)$$

The solution is

$$\hat{\alpha}_j = \mathbf{z}_j + \frac{\lambda_j}{2} < 0. \quad (9)$$

108 So $\mathbf{z}_j < -\frac{\lambda_j}{2} < 0$, and the solution $\hat{\alpha}_j$ can be written as
 109

$$\hat{\alpha}_j = \text{sgn}(\mathbf{z}_j) * (-\mathbf{z}_j - \frac{\lambda_j}{2}) = \text{sgn}(\mathbf{z}_j) * (|\mathbf{z}_j| - \frac{\lambda_j}{2}). \quad (10)$$

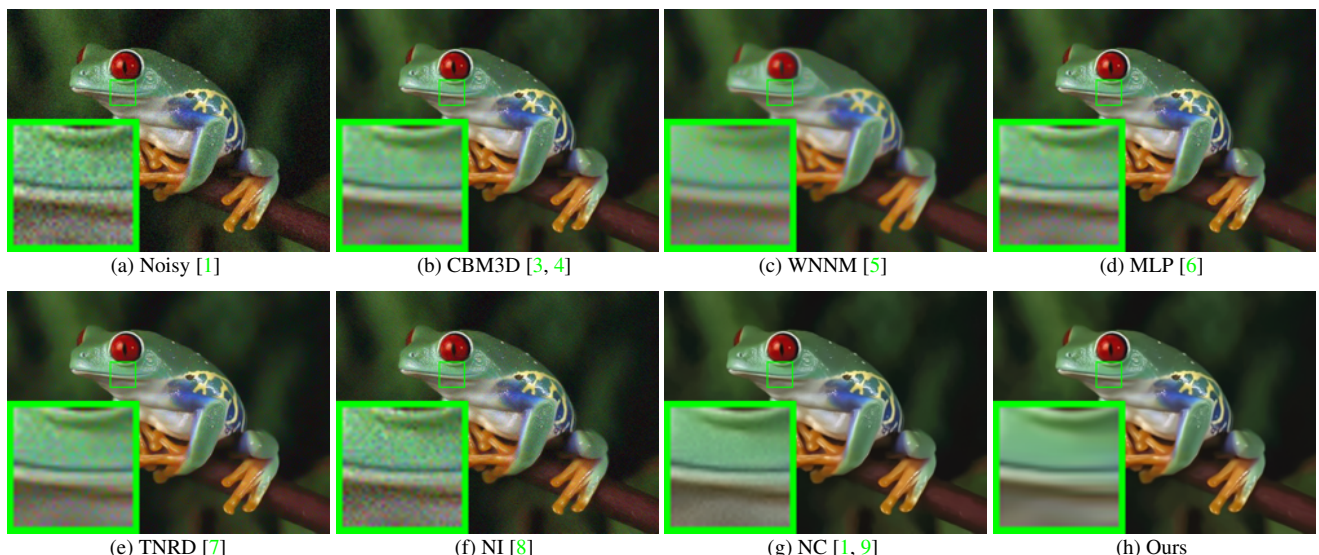
110 In summary, we have the final solution of the weighted sparse coding problem (1) as
 111

$$\hat{\alpha} = \text{sgn}(\mathbf{D}^T \mathbf{y}) \odot \max(|\mathbf{D}^T \mathbf{y}| - \boldsymbol{\lambda}, 0), \quad (11)$$

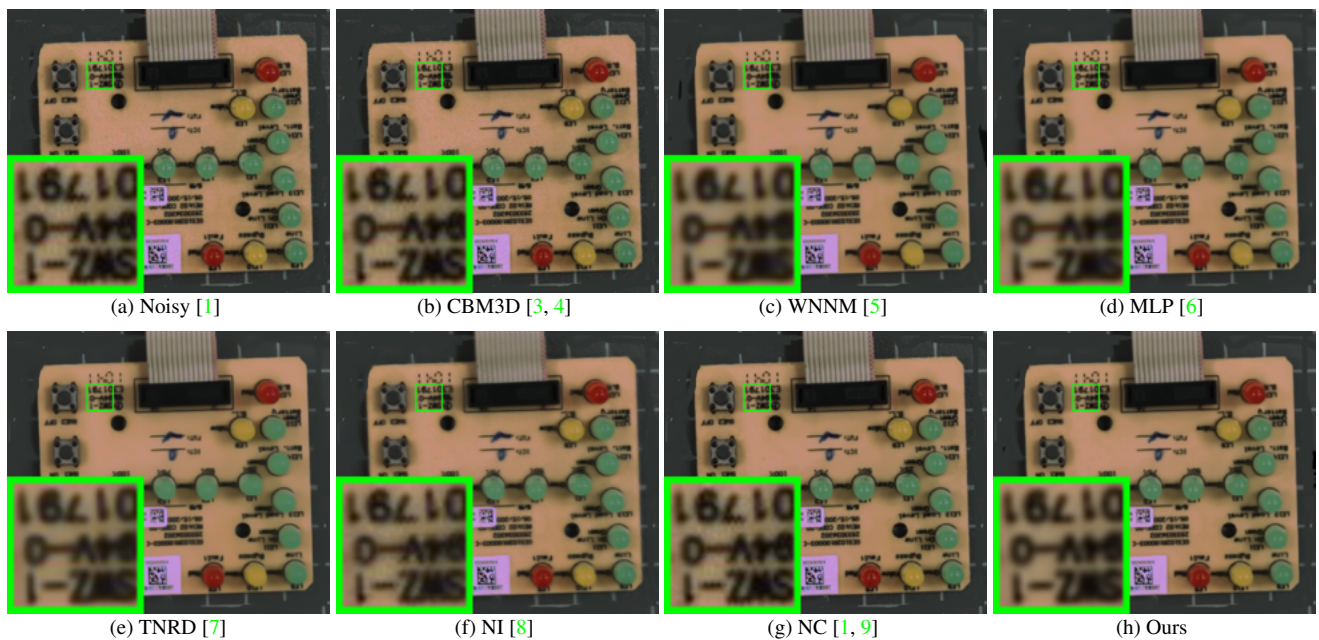
112 where $\boldsymbol{\lambda} = \frac{1}{2}[\lambda_1, \lambda_2, \dots, \lambda_{3p^2}]^\top$ is the vector of regularization parameter and \odot means element-wise multiplication.
 113

114 2. More Results on Real Noisy Images in [1]

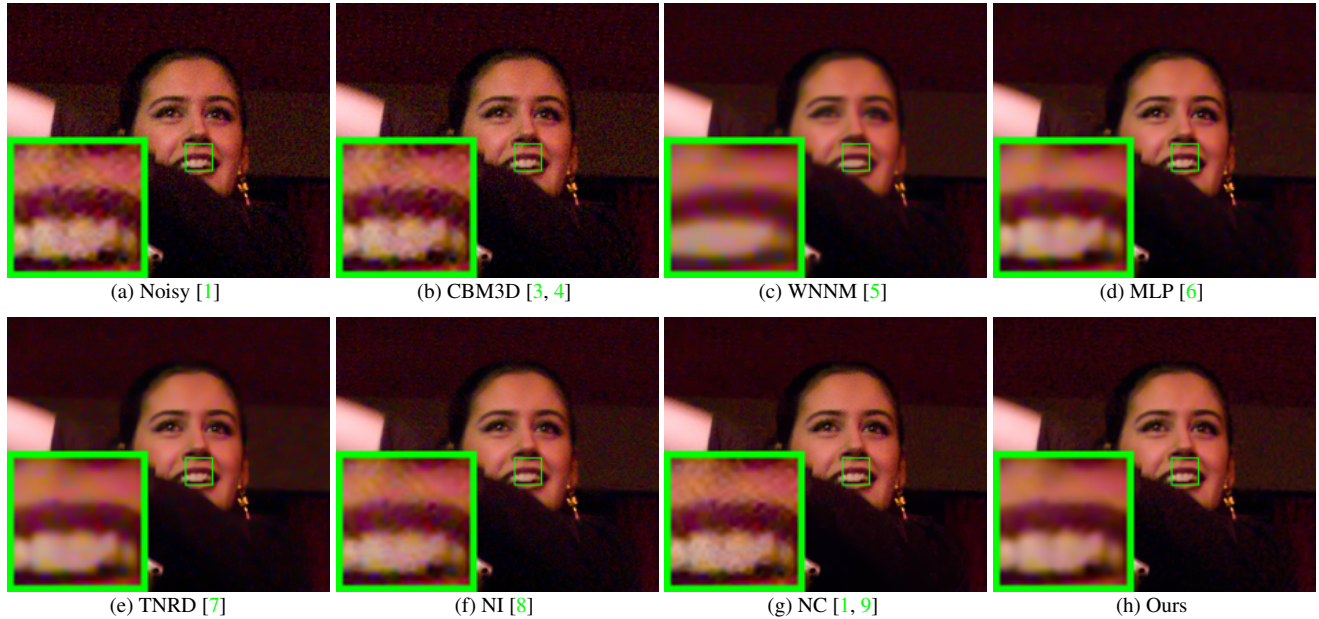
115 In this section, we give more comparisons of the competing methods on the dataset [1]. The real noisy images in dataset [1]
 116 have no “ground truth” images and hence we only compare the visual quality of the denoised images by different methods.
 117 As can be seen from Figures 1-4, our proposed method performs better than the state-of-the-art denoising methods.
 118



119 Figure 1. Denoised images of the real noisy image “Frog” [1] by different methods. The images are better to be zoomed in on screen.
 120



121 Figure 2. Denoised images of the real noisy image “Circuit” [1] by different methods. The images are better to be zoomed in on screen.
 122

216
217
218
219
220
221
222
223
224
225
226227 Figure 3. Denoised images of the real noisy image “Woman” [1] by different methods. The images are better to be zoomed in on screen.
228

229

230

231

232

233

234

235

236

237

238

239

240

241

242

243

244

245

246

247

248

249

250

251

252

253

254

255

256

257

258

259

260

261

262

263

264

265

266

267

268

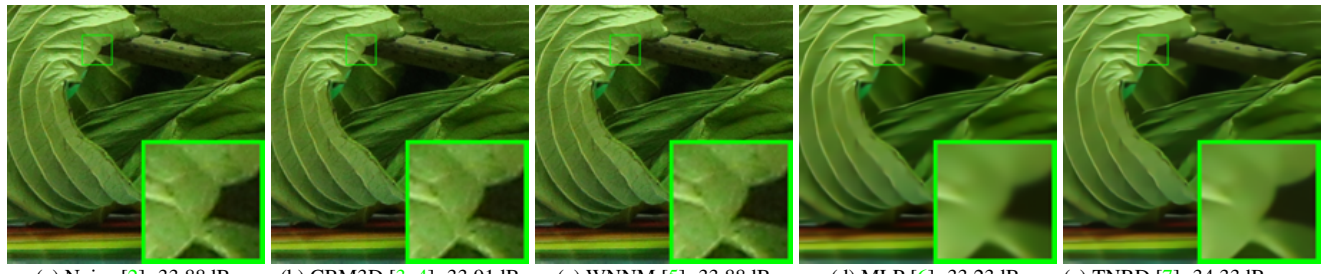
269

270
271
272
273
274
275
276
277
278
279
280
281
282
283
284
285
286
287
288
289
290
291
292
293
294
295
296
297
298
299
300
301
302
303
304
305
306
307
308
309
310
311
312
313
314
315
316
317
318
319
320
321
322
323299 Figure 4. Denoised images of the real noisy image “Vehicle” [1] by different methods. The images are better to be zoomed in on screen.
300

3. More Results on the 15 Cropped Images Used in [2]

In this section, we provide more visual comparisons of the proposed method with the state-of-the-art denoising methods on the 15 cropped real noisy images used in [2]. As can be seen from Figures 5-9, on most cases, our proposed method achieves better performance than the competing methods. This validates the effectiveness of our proposed external prior guided internal prior learning framework for real noisy image denoising.

324



378

379

380

381

382

383

384

385

386

387

388

389

390

391

392

393

394

395

396

397

398

399

400

Figure 5. Denoised images of a region cropped from the real noisy image “Canon 5D Mark 3 ISO 3200 2” [2] by different methods. The images are better to be zoomed in on screen.

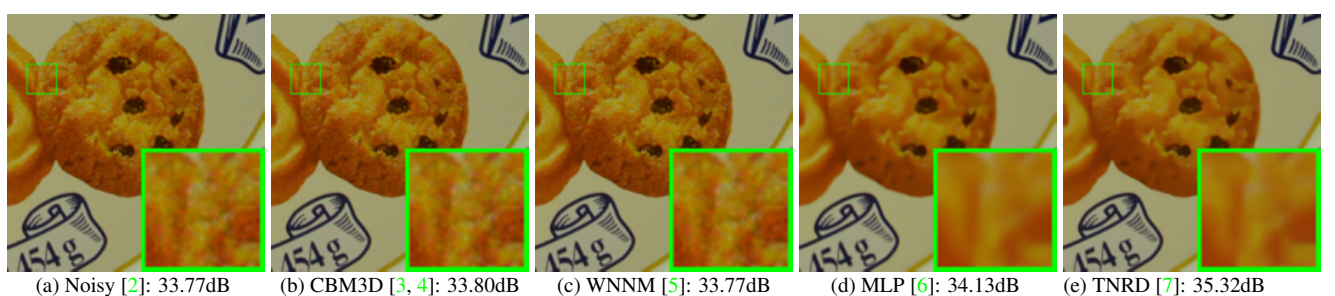
343

344

345

346

347



401

402

403

404

405

406

407

408

409

410

411

412

413

414

415

416

417

418

419

356

357

358

359

360

361

362

363

364

365

366

367

368

369

370

371

372

373

374

375

376

377

Figure 6. Denoised images of a region cropped from the real noisy image “Canon 5D Mark 3 ISO 3200 2” [2] by different methods. The images are better to be zoomed in on screen.

420

421

422

423

424

425

426

427

428

429

430

431

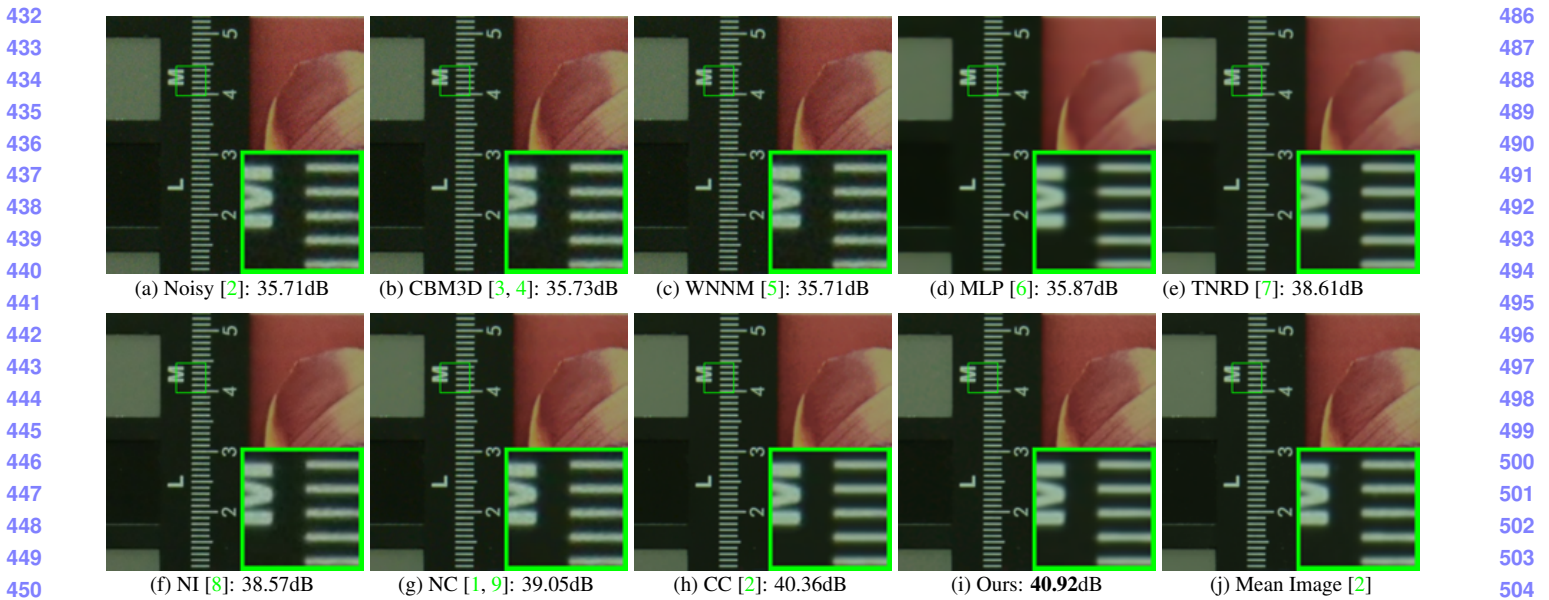


Figure 7. Denoised images of a region cropped from the real noisy image “Nikon D800 ISO 1600 2” [2] by different methods. The images are better to be zoomed in on screen.

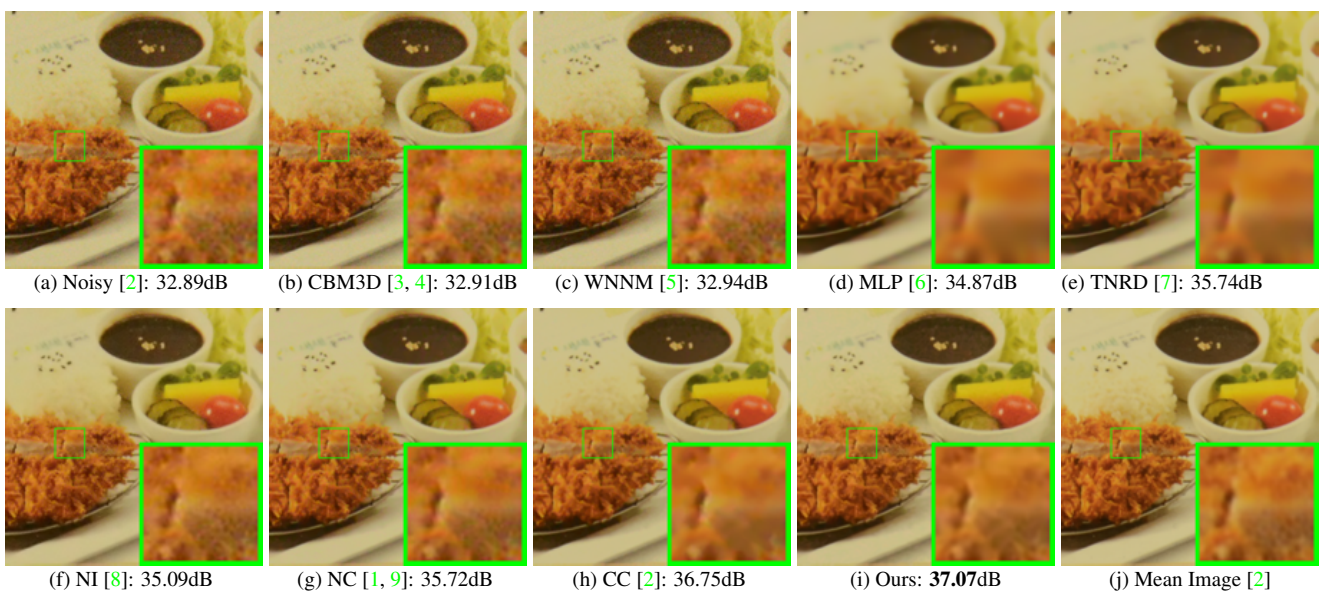


Figure 8. Denoised images of a region cropped from the real noisy image “Nikon D800 ISO 3200 2” [2] by different methods. The images are better to be zoomed in on screen.

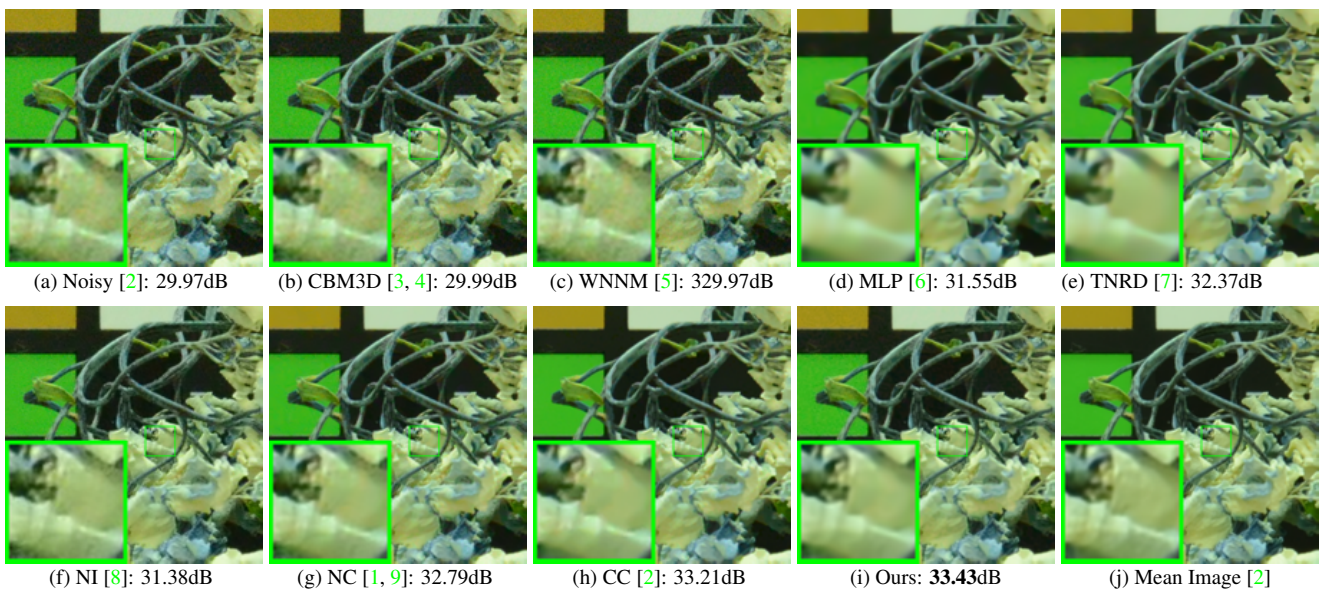


Figure 9. Denoised images of a region cropped from the real noisy image “Nikon D800 ISO 6400 2” [2] by different methods. The images are better to be zoomed in on screen.

4. More Results on the 60 Cropped Images in [2]

In this section, we provide more visual comparisons of the proposed method with the state-of-the-art denoising methods on the 60 cropped real noisy images we cropped from [2]. As can be seen from Figures 10-20, on most cases, our proposed method achieves better performance than the competing methods. This validates the effectiveness of our proposed external prior guided internal prior learning framework for real noisy image denoising.

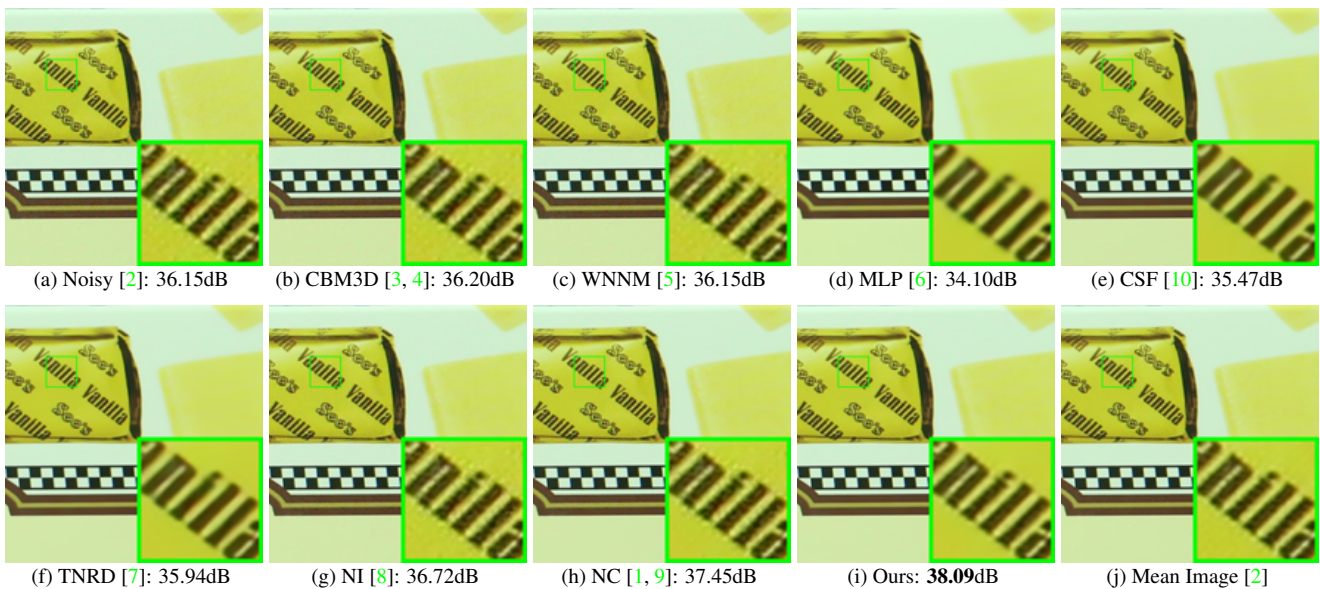


Figure 10. Denoised images of a region cropped from the real noisy image “Canon EOS 5D Mark3 ISO 3200 C1” [2] by different methods. The images are better viewed by zooming in on screen.

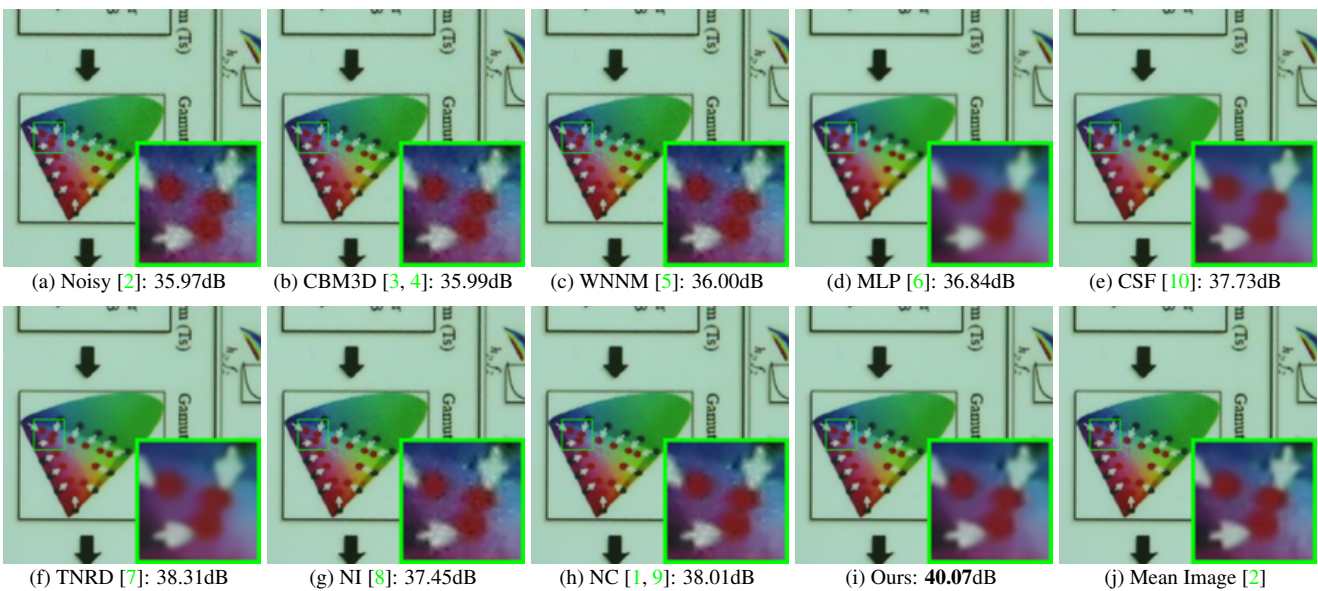


Figure 11. Denoised imagesupp of a region cropped from the real noisy image “Canon EOS 5D Mark3 ISO 3200 C2” [2] by different methods. The images are better viewed by zooming in on screen.

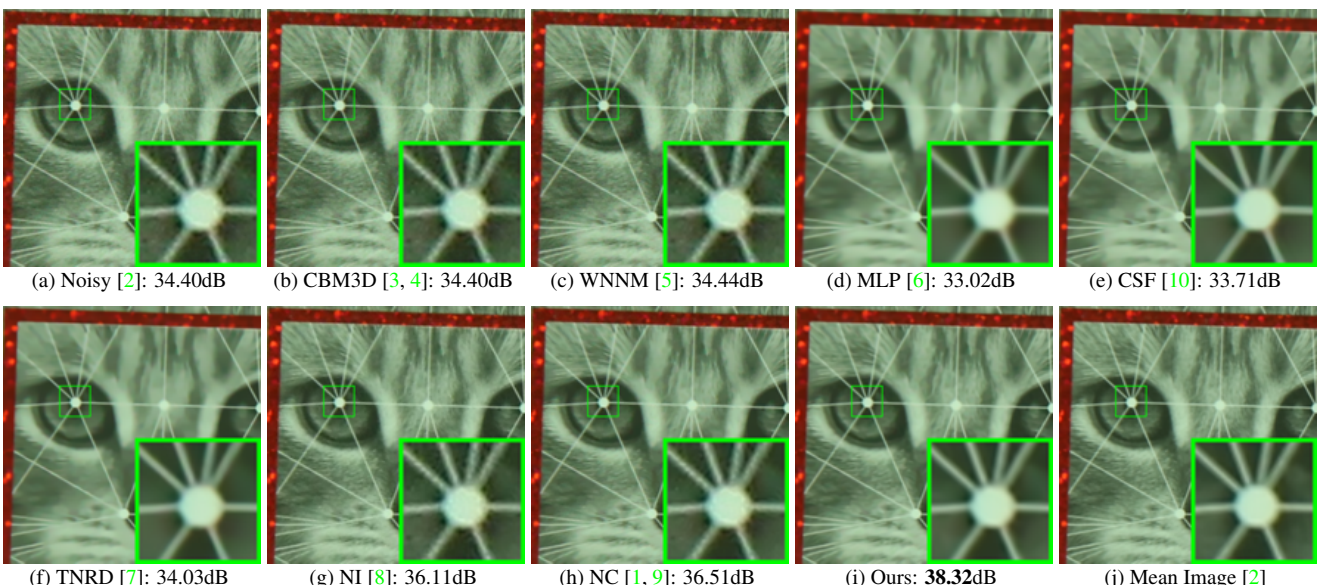


Figure 12. Denoised imagesupp of a region cropped from the real noisy image “Canon EOS 5D Mark3 ISO 3200 C3” [2] by different methods. The images are better viewed by zooming in on screen.

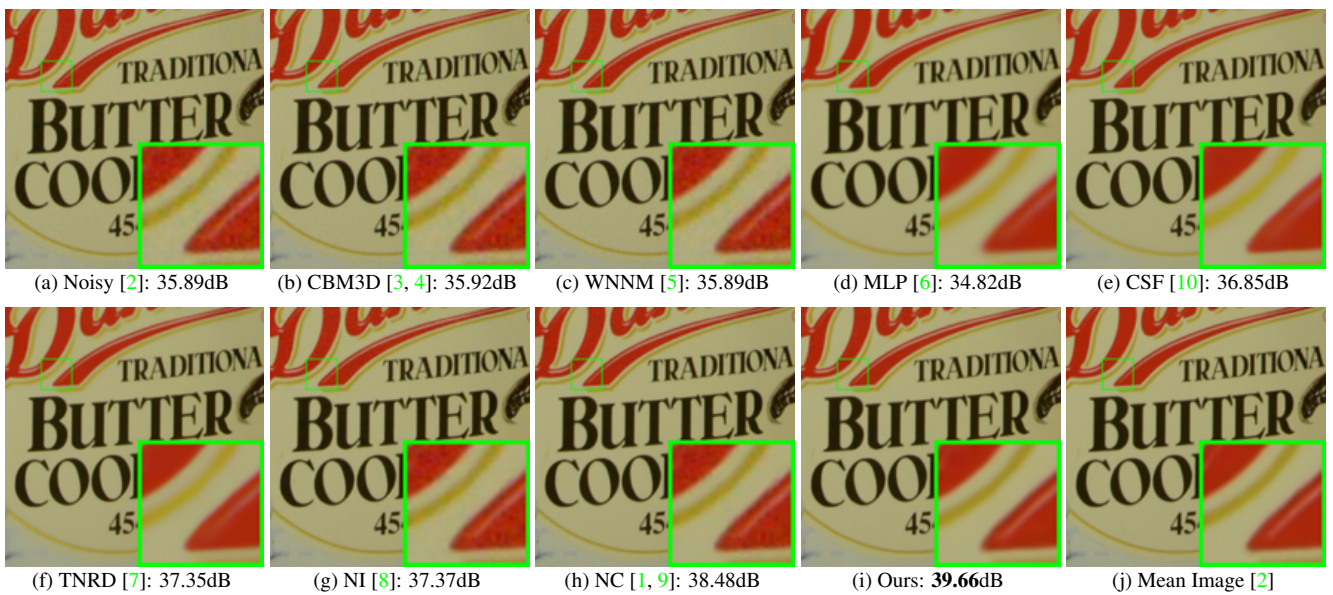


Figure 13. Denoised imagesupp of a region cropped from the real noisy image “Nikon D600 ISO 3200 C1” [2] by different methods. The images are better viewed by zooming in on screen.

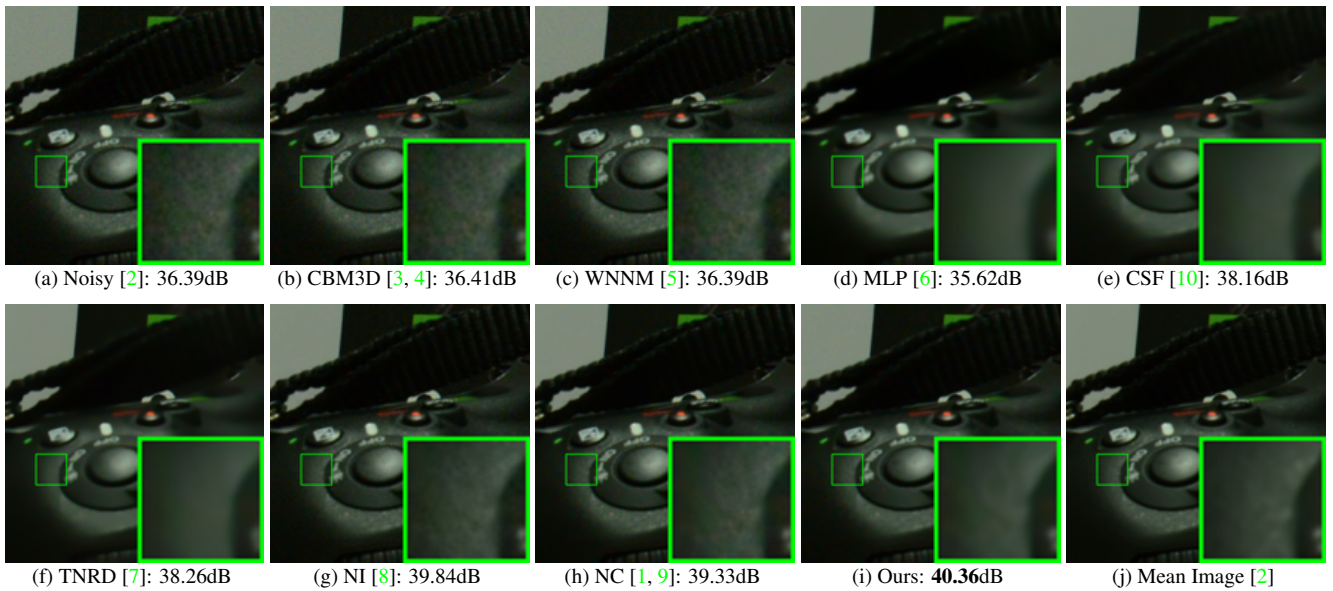


Figure 14. Denoised imagesupp of a region cropped from the real noisy image “Nikon D600 ISO 3200 C2” [2] by different methods. The images are better viewed by zooming in on screen.

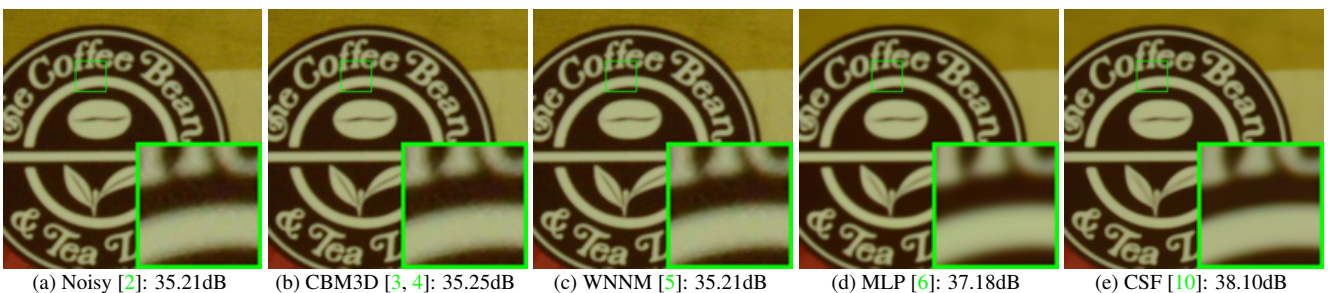


Figure 15. Denoised imagesupp of a region cropped from the real noisy image “Nikon D800 ISO 1600 B2” [2] by different methods. The images are better viewed by zooming in on screen.

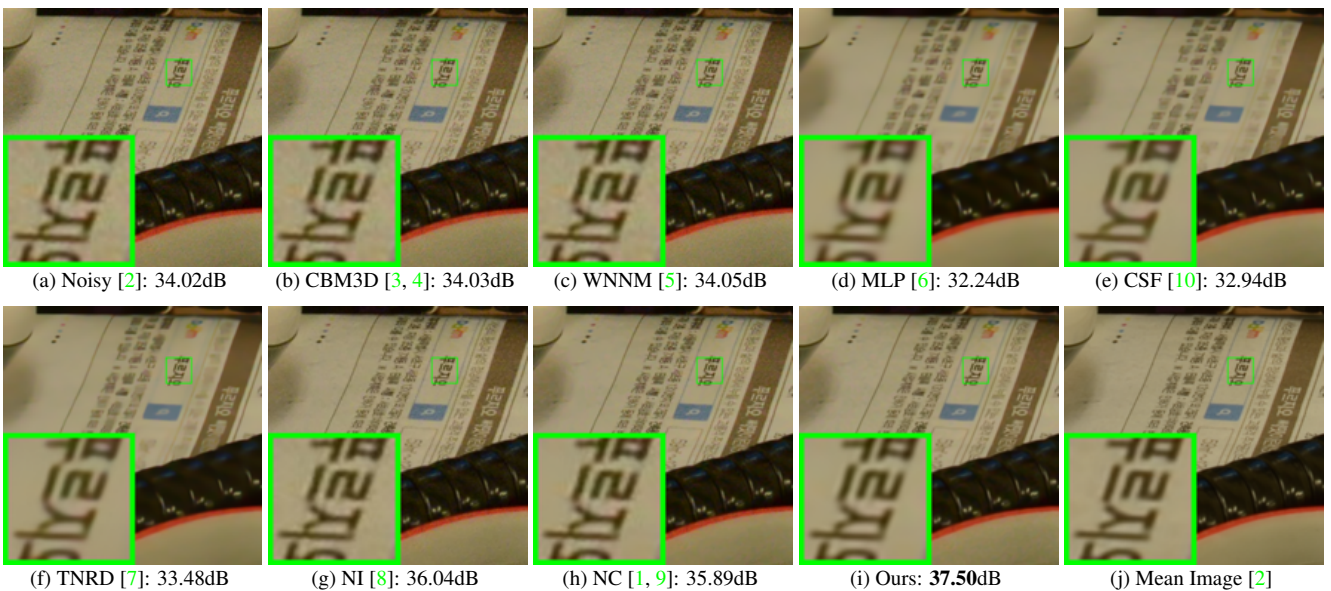


Figure 16. Denoised imagesupp of a region cropped from the real noisy image “Nikon D800 ISO 3200 A1” [2] by different methods. The images are better viewed by zooming in on screen.

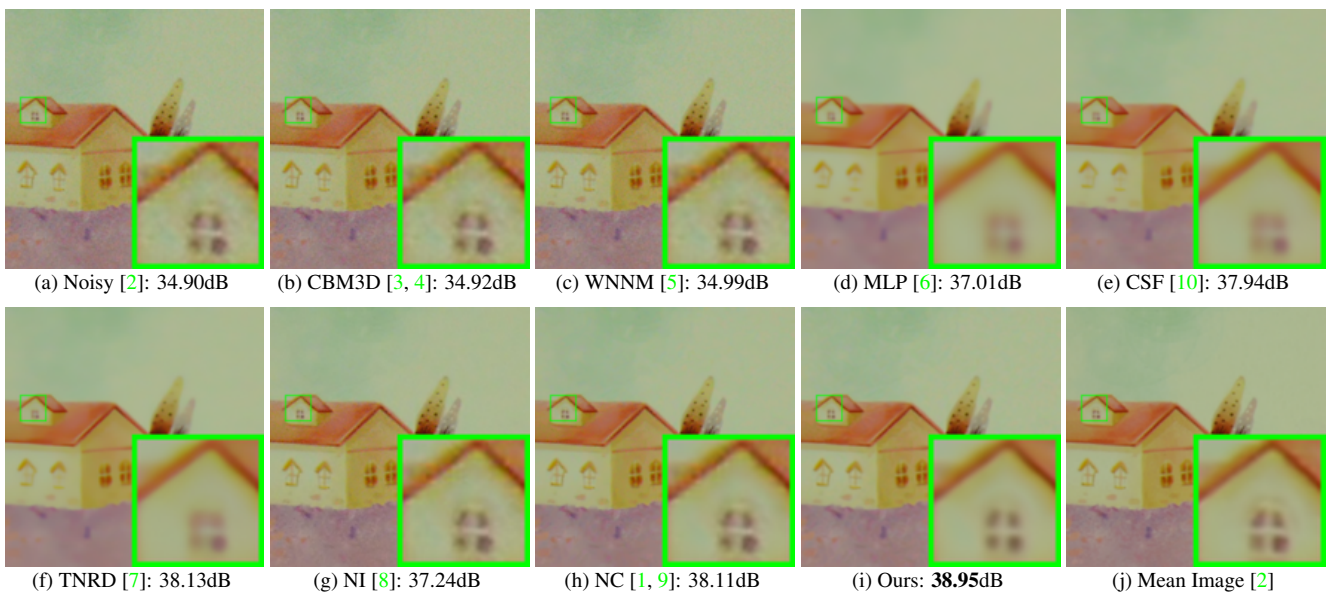


Figure 17. Denoised imagesupp of a region cropped from the real noisy image “Nikon D800 ISO 3200 A2” [2] by different methods. The images are better viewed by zooming in on screen.

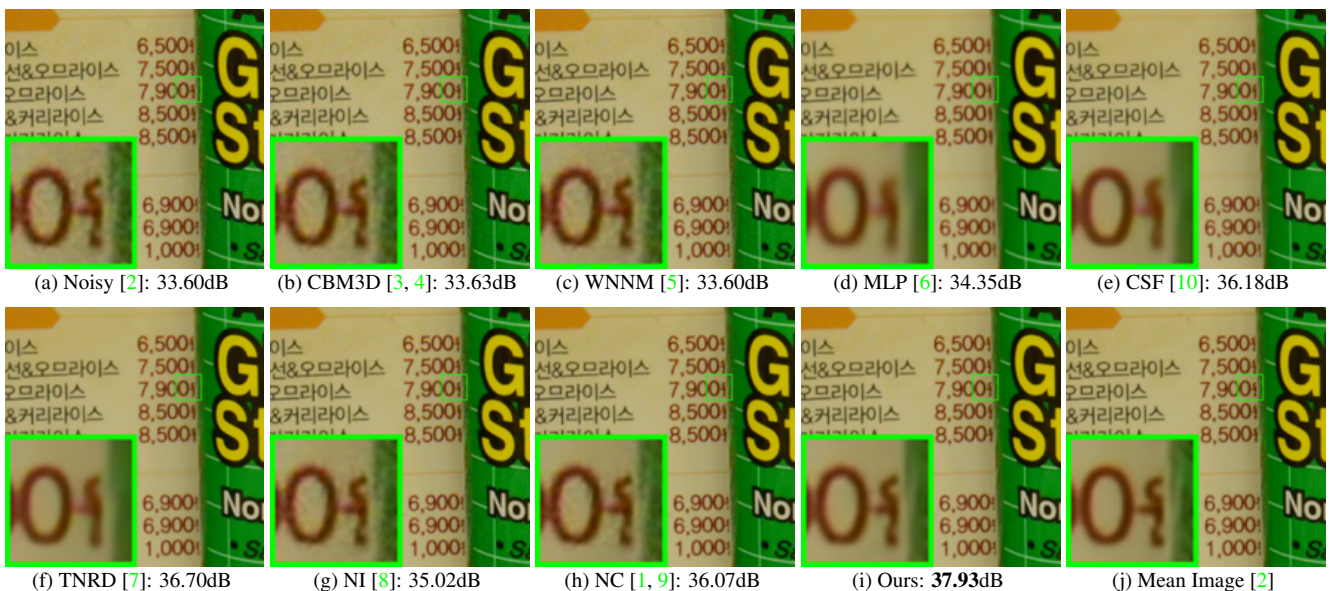


Figure 18. Denoised imagesupp of a region cropped from the real noisy image “Nikon D800 ISO 3200 A3” [2] by different methods. The images are better viewed by zooming in on screen.

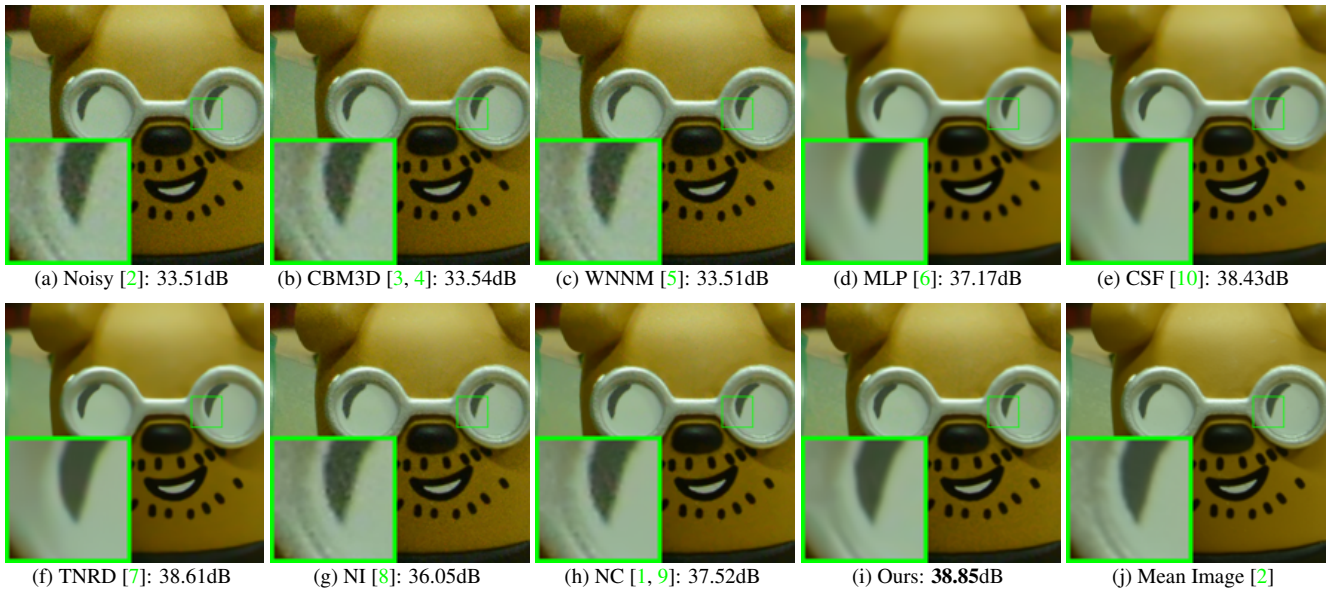


Figure 19. Denoised imagesupp of a region cropped from the real noisy image “Nikon D800 ISO 3200 A4” [2] by different methods. The images are better viewed by zooming in on screen.

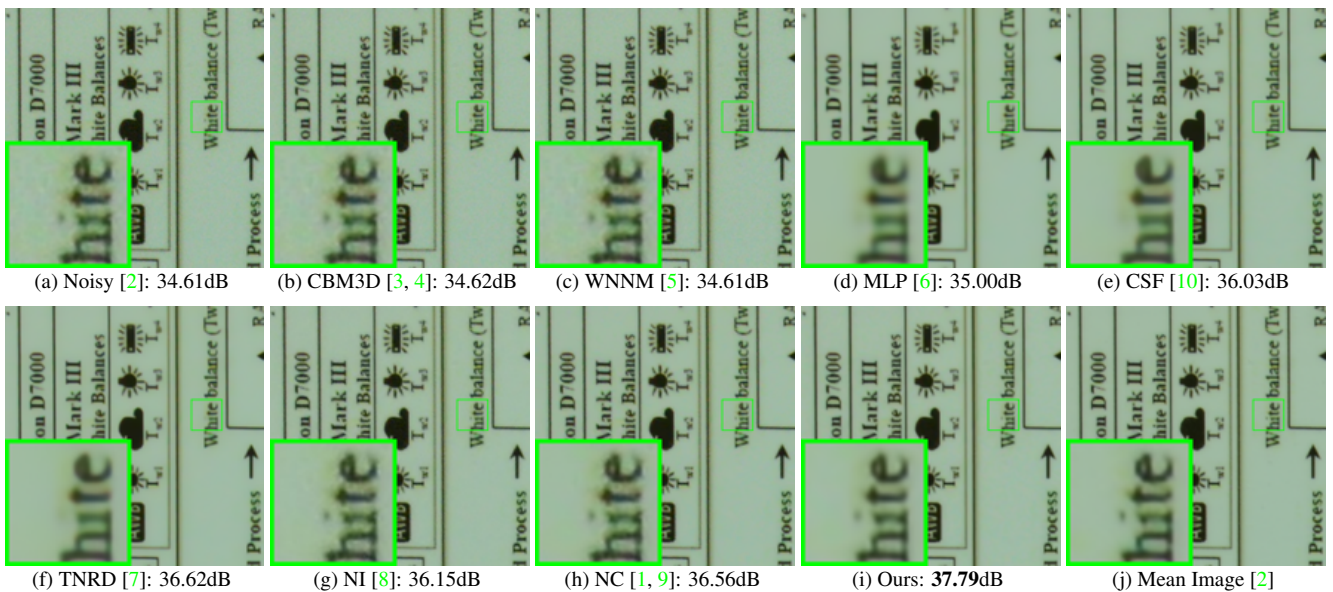


Figure 20. Denoised imagesupp of a region cropped from the real noisy image “Nikon D800 ISO 3200 A5” [2] by different methods. The images are better viewed by zooming in on screen.

References

- [1] M. Lebrun, M. Colom, and J. M. Morel. The noise clinic: a blind image denoising algorithm. <http://www.ipol.im/pub/art/2015/125/>. Accessed 01 28, 2015. 1, 2, 3, 4, 5, 6, 7, 8, 9, 10, 11
- [2] S. Nam, Y. Hwang, Y. Matsushita, and S. J. Kim. A holistic approach to cross-channel image noise modeling and its application to image denoising. *IEEE Conference on Computer Vision and Pattern Recognition (CVPR)*, pages 1683–1691, 2016. 1, 3, 4, 5, 6, 7, 8, 9, 10, 11
- [3] K. Dabov, A. Foi, V. Katkovnik, and K. Egiazarian. Image denoising by sparse 3-D transform-domain collaborative filtering. *IEEE Transactions on Image Processing*, 16(8):2080–2095, 2007. 2, 3, 4, 5, 6, 7, 8, 9, 10, 11

- 1188 [4] K. Dabov, A. Foi, V. Katkovnik, and K. Egiazarian. Color image denoising via sparse 3D collaborative filtering with grouping 1242
1189 constraint in luminance-chrominance space. *IEEE International Conference on Image Processing (ICIP)*, pages 313–316, 2007. 2, 1243
1190 3, 4, 5, 6, 7, 8, 9, 10, 11 1244
- 1191 [5] S. Gu, L. Zhang, W. Zuo, and X. Feng. Weighted nuclear norm minimization with application to image denoising. *IEEE Conference 1245
1192 on Computer Vision and Pattern Recognition (CVPR)*, pages 2862–2869, 2014. 2, 3, 4, 5, 6, 7, 8, 9, 10, 11 1246
- 1193 [6] H. C. Burger, C. J. Schuler, and S. Harmeling. Image denoising: Can plain neural networks compete with BM3D? *IEEE Conference 1247
1194 on Computer Vision and Pattern Recognition (CVPR)*, pages 2392–2399, 2012. 2, 3, 4, 5, 6, 7, 8, 9, 10, 11 1248
- 1195 [7] Y. Chen, W. Yu, and T. Pock. On learning optimized reaction diffusion processes for effective image restoration. *IEEE Conference 1249
1196 on Computer Vision and Pattern Recognition (CVPR)*, pages 5261–5269, 2015. 2, 3, 4, 5, 6, 7, 8, 9, 10, 11 1250
- 1197 [8] Neatlab ABSoft. Neat Image. <https://ni.neatvideo.com/home>. 2, 3, 4, 5, 6, 7, 8, 9, 10, 11 1251
- 1198 [9] M. Lebrun, M. Colom, and J.-M. Morel. Multiscale image blind denoising. *IEEE Transactions on Image Processing*, 24(10):3149– 1253
1199 3161, 2015. 2, 3, 4, 5, 6, 7, 8, 9, 10, 11 1254
- 1200 [10] U. Schmidt and S. Roth. Shrinkage fields for effective image restoration. *IEEE Conference on Computer Vision and Pattern Recog- 1255
1201 nition (CVPR)*, pages 2774–2781, June 2014. 6, 7, 8, 9, 10, 11 1256
- 1202
- 1203
- 1204
- 1205
- 1206
- 1207
- 1208
- 1209
- 1210
- 1211
- 1212
- 1213
- 1214
- 1215
- 1216
- 1217
- 1218
- 1219
- 1220
- 1221
- 1222
- 1223
- 1224
- 1225
- 1226
- 1227
- 1228
- 1229
- 1230
- 1231
- 1232
- 1233
- 1234
- 1235
- 1236
- 1237
- 1238
- 1239
- 1240
- 1241